Available online at www.sciencedirect.com
SCIENCE DIRECT®
Journal of Solid State Chemistry 178 (2005) 661–670
JOURNAL OF SOLID STATE CHEMISTRY
www.elsevier.com/locate/jssc

On the precipitation of coherent spinel nanoparticles in Ti-doped MgO

K.C. Yang, P. Shen*

Institute of Materials Science and Engineering, National Sun Yat-sen University, Number 70, Lien-Hai Road, Kaohsiung, Taiwan, ROC

Received 17 October 2004; received in revised form 8 December 2004; accepted 10 December 2004

Abstract

The Mg_2TiO_4/MgO composites prepared by reactive sintering of MgO and TiO_2 powders (9:1 molar ratio) at 1600 °C and then air-cooled or further aged at 900 °C were studied by X-ray diffraction and analytical electron microscopy in order to characterize the microstructures and formation mechanism of nanosized Mg_2TiO_4 spinel precipitated from Ti-doped MgO. Expulsion of Ti^{4+} during cooling caused the formation of (001)-specific Guinier–Preston zone under the influence of thermal/sintering stress and then the spinel precipitates, which were about 30 nm in size and nearly spherical with {111} and {100} facets to minimize coherency strain energy and surface energy. Secondary nanosized spinel was precipitated and became site saturated during aging at 900 °C, leaving a precipitate-free zone at the grain boundaries of Ti-doped MgO. The intergranular spinel became progressively Ti-richer upon aging at 900 °C and showed ⟨110⟩-specific diffuse scatter intensity likely due to short-range ordering and/or onset decomposition.

Keywords: Ti-doped MgO; Spinel; Coherent nanoparticle; Intermediate phase; AEM

1. Introduction

The MgO–TiO_2 phase diagram [1,2] indicated that the cubic close-packed (CCP) monoxide of rock-salt structure, i.e., periclase MgO, has negligible solid solubility of Ti. However, we report here that nanosized Mg_2TiO_4 with inverse spinel structure (space group $Fd3m$) was exsolved from Ti-doped MgO via a metastable intermediate. We focused on the competitive factors of coherency strain and defect clustering for forming the Guinier–Preston (G.P.) zone, rather than paracrystalline distribution of defect clusters. Besides, the controlled nucleation and growth of the precipitates as a result of site saturation at specific undercooling was studied.

The G.P. zone, a fully coherent precipitate, commonly occurs as metastable intermediate in the early stages of many precipitation processes [3]. For example, expulsion of Zr^{4+} in Zr-doped α-Fe_2O_{3-x} (hematite) caused the formation of G.P. zones and then disk-like iron zirconate precipitates [4]. The orientation of G.P. zones can be stress induced as observed in early stage precipitation of Al–Cu alloy [5].

On the other hand, 3D transition metal CCP monoxides, with varied extent of nonstoichiometry and doping of aliovalent cations, commonly form paracrystalline distribution of defect clusters before the precipitation of spinel oxide. The paracrystalline distribution is such that the spacing between defects remains fairly constant but the relative lateral translation may occur more variably [6]. $Fe_{1-x}O$ having a considerable degree of nonstoichiometry ($x<0.15$ [7]) was known to possess defect clusters of 4:1 type with four octahedral vacant sites surrounding one Fe^{3+}-filled tetrahedral interstitial site [8]. When aged at high temperatures, the 4:1 clusters may assemble into larger units (e.g., 13:4, 16:5 and form a paracrystal [6,9]), which order further into Fe_3O_4 spinel or other ordered phases: p'' and p''' [10,11]. For $Ni_{1-x}O$ with a very small x (ca. 0.001 at 1500 °C [12]), there is still significant

*Corresponding author. Fax: +886 7 525 4099.
E-mail address: pshen@mail.nsysu.edu.tw (P. Shen).

0022-4596/$ - see front matter © 2004 Elsevier Inc. All rights reserved.
doi:10.1016/j.jssc.2004.12.019

defect clustering when Zr doped or (Zr, *Y*) co-doped [13,14]. (The Zr-doped or (Zr, *Y*) co-doped $Ni_{1-x}O$ transformed into a paracrystal and then Ni_3O_4 spinel when annealed at 1300 or 1600 °C [13,14].) In the case of $Co_{1-x}O$ with a moderate x (ca. 0.01 [15]), spontaneous oxidation to form Co_3O_4 spinel was known to occur by cooling below 900 °C [16]. Paracrystal intermediate and then spinel phase, however form above 900 °C for (Zr, *Y*) co-doped $Co_{1-x}O$ [17]. The $Co_{3-\delta}O_4$ spinel also formed paracrystals [18].

Here, we used the fired MgO/Mg_2TiO_4 composite to study whether Ti-doped MgO formed G.P. zones or paracrystals in the nascent precipitation stage. In our previous study of analog $Ni_{1-x}O/NiAl_2O_4$ composite, the platelets of inverse spinel $NiAl_2O_4$ were found to nucleate rapidly at dislocations of the Al^{3+}-doped $Ni_{1-x}O$ and there appeared to be no intermediate paracrystalline state [19]. MgO/Mg_2TiO_4 is a more refractory and less solid soluble composite than $Ni_{1-x}O/NiAl_2O_4$ for an interesting comparison of precipitation behavior. We emphasized on the formation of (001)-specific G.P. zone under the influence of thermal/sintering stress and the controlled nucleation and growth of coherent nanosized Mg_2TiO_4 spinel precipitates from Ti-doped MgO. In addition, the combined effects of a rather limited solid solubility, site saturation and strain/surface energetics on precipitation behavior were discussed. Furthermore, Mg_2TiO_4 shows significant cation disordering above 900 °C [20], eutectoid decomposition to $MgTiO_3$ (ilmenite structure) plus MgO upon prolonged annealing near 900 °C [2], and possible distortion into tetragonal symmetry (space group $P4_122$) below 664 °C [21]. The characterization of defects in the present intra/intergranular Mg_2TiO_4 would shed light on these processes. The microstructure development of the present composites would also be an interesting comparison with the precipitation of spinel in titanium-doped MgO single crystals in the temperature range of 1100–1500 °C [22] and the sintering of $MgO–TiO_2$ in the range of 1300–1600 °C [23]. By the controlled nucleation and growth following a reactive sintering and then annealing route, we demonstrated that metal oxide precipitates can be tailored as nanosize particles for potential applications as heterogeneous catalysts.

2. Experimental

The MgO (99.9%, Cerac) and TiO_2 (99.9%, Cerac) powders in 9:1 molar ratio were mixed by a magnetic stirrer in ethanol at 50 °C for 2 h, oven-dried at 70 °C and then ground with an agate mortar and pestle. The powder mixture was then die pressed at 650 MPa to form pellets ca. 5 mm in diameter and 2 mm in thickness. The pellets were reaction sintered at 1600 °C for 4 and 24 h in an open-air furnace to form MgO/Mg_2TiO_4 composite and cooled outside the furnace. The pellets fired at 1600 °C for 4 h were further aged at 900 °C for 5 and 30 h in an open-air furnace and cooled outside the furnace.

X-ray diffraction (XRD, Cu$K\alpha$, 40 kV, 30 mA at 0.05° and 3 s/step within 2θ angles 15–110°) was used to identify the phases. The *d*-spacings measured from XRD trace were used for least-squares refinement of the lattice parameters. (The program UnitCell by T.J.B. Holland and S.A.T. Redfern (1995) was used for the refinement of lattice parameters.) The error of the *d*-spacing measurements on XRD trace and the calculated lattice parameters were estimated to be accurate within ± 0.0002 nm for the predominant Ti-doped MgO and ± 0.0003 nm for minor spinel phase.

The fired MgO/Mg_2TiO_4 composites were argon-ion milled to electron transparency and studied by analytical electron microscopy (AEM) using JEOL 3010 instrument at 300 kV for imaging and energy-dispersive X-ray (EDX) analysis. The EDX analysis was performed using *K* shell counts for Mg and Ti, and the principle of ratio method without absorption correction [24]. Bright field image (BFI), dark field image (DFI), high-resolution transmission electron microscopy (HRTEM) image and selected area electron diffraction (SAED) pattern were taken to identify phases and defects. Scanning electron microscopy (SEM, JSM-6400 at 20 kV) was used to study the thermally etched (1500 °C for 10 min) surface of the fired specimens.

3. Results

3.1. XRD

Rock-salt- and spinel-type oxides were identified by XRD for the specimens fired at 1600 °C for 4 and 24 h (Figs. 1a and b) and further aged at 900 °C for 5 and 30 h (Figs. 1c and d). Regardless of firing temperature and time, the rock-salt-type oxide was MgO doped with nearly the same amount of Ti^{4+} as indicated by a nearly constant room-temperature lattice parameter (0.4208 ± 0.0002 nm) which appeared to be slightly smaller than undoped MgO (0.4211 nm, JCPDS file 45-0946). It should be noted, however, that the maximum Ti content in MgO was determined as 0.3 wt% [23]. On the basis of the mean metal–oxygen distance for magnesium titanates in general [25], the lattice parameter of MgO with 0.3 wt% Ti would shrink for about 0.00004 nm, which is one order of magnitude lower than the uncertainty of the present XRD. It is therefore not justified to estimate the Ti content in MgO from the present lattice parameter measurements. On the other hand, the interpretation of lower lattice constant due to Ti dopant is more capable for the

spinel, which is more variable in stoichiometry than MgO. In fact, the Ti-doped MgO showed no appreciable change of lattice parameter upon aging at 900 °C in spite of a slight expulsion of Ti^{4+} to form minute amounts of spinel precipitates as revealed by AEM. In contrast, the spinel has a slightly smaller lattice parameter with firing time, i.e., 0.8423 and 0.8417 ± 0.0003 nm for the samples fired at 1600 °C for 4 and 24 h, respectively, and then 0.8415 and 0.8412 ± 0.0003 nm for the samples fired at 900 °C for 5 and 30 h, respectively. This indicates that the spinel nucleus formed by reactive sintering has a composition close to stoichiometric Mg_2TiO_4 (0.8441 nm, JCPDS file 25-1157), whereas the spinel aged at 900 °C is Ti richer and hence has a shorter mean metal–oxygen distance analogous to magnesium titanates in general [25].

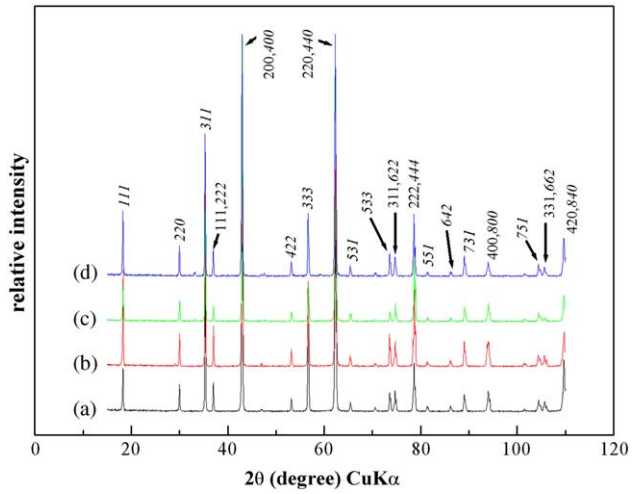

Fig. 1. XRD traces of reactively sintered MgO/Mg_2TiO_4 composites: (a,b) fired at 1600 °C for 4 and 24 h, respectively; (c,d) subject to further annealing at 900 °C for 5 and 30 h, respectively, followed by air quenching. Note diffraction peaks of Ti-doped MgO (*hkl*) with rock-salt structure and Mg_2TiO_4 (italic (*hkl*)) with inverse spinel structure.

3.2. SEM

The fired composites showed inter- and intragranular particles of both MgO (dark) and Mg_2TiO_4 (bright) phases (Fig. 2). (Inter- and intragranular Mg_2TiO_4 were also reported to form in the MgO when added up to 10 wt% TiO_2 and sintered above 1300 °C [23].) Due to dragging of intergranular particles, there is a rather limited growth of the host grains from 4 to 24 h at 1600 °C (Fig. 2a and 2b) and upon further annealing at 900 °C for 5 and 30 h (Fig. 2c and 2d). The 120° grain junctions indicated a solid-state reactive sintering process at 1600 °C, which is slightly below the eutectic temperatures (1605 and 1630 °C) of the MgO–TiO_2 binary [1].

3.3. TEM

3.3.1. Precipitates in Ti-doped MgO

The composite fired at 1600 °C for 4 h and then cooled in air showed homogeneous precipitates of Mg_2TiO_4 spinel (denoted as S) in Ti-doped MgO (rock-salt type denoted as R) (Fig. 3a). The two phases followed parallel epitaxial relationship, i.e., $[112]_R \| [112]_S$; $(1\bar{1}0)_R \| (1\bar{1}0)_S$ as indicated by SAED pattern. This relationship is the same as that reported for the

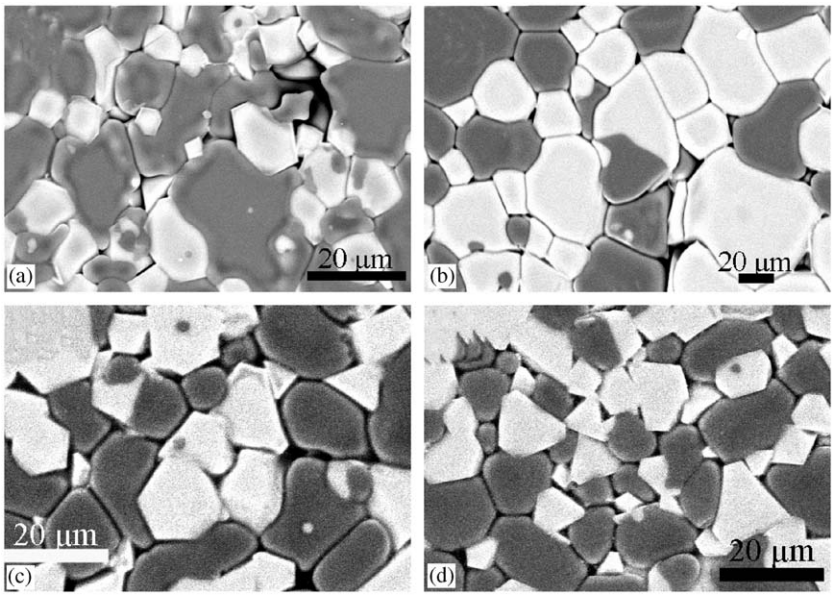

Fig. 2. SEM image (secondary electron image) of reactively sintered MgO/Mg_2TiO_4 composites: (a,b) fired at 1600 °C for 4 and 24 h, respectively; (c,d) subject to further annealing at 900 °C for 5 and 30 h, respectively. *Note*: samples were thermally etched at 1500 °C for 10 min to show grain boundaries and inter/intragranular particles of MgO (dark) and Mg_2TiO_4 (bright).

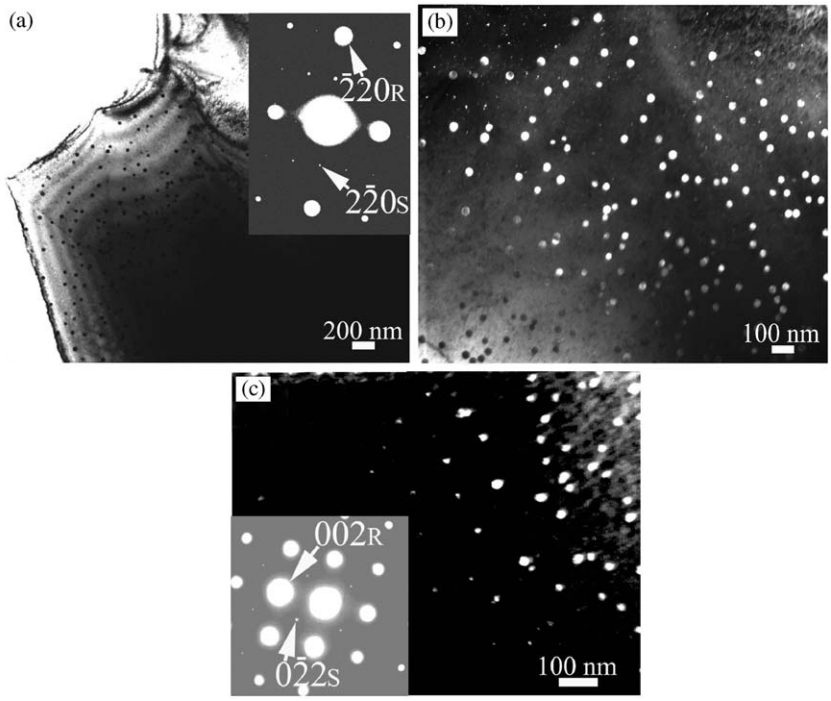

Fig. 3. TEM (a) BFI with inset SAED pattern in [112] zone axis showing homogeneous precipitates of parallel epitaxial spinel (denoted as S) in Ti-doped MgO (denoted as R) for sample fired at 1600 °C for 4 h. (b) DFI ($g = \bar{2}20$ spinel) of local area in (a) showing slightly faceted precipitates ca. 30 nm in size. (c) DFI ($g = 022$ spinel) with inset SAED pattern ([100] zone axis) showing negligible change of precipitate size when subject to further annealing at 1600 °C for 24 h.

precipitation in MgO single crystals [22]. DFI using spinel diffraction (Fig. 3b) indicated that the spinel precipitates are about 30 nm in size and slightly faceted. There is negligible change of precipitate size and orientation when subject to further dwelling at 1600 °C for up to 24 h (Fig. 3c), indicating that the spinel was precipitated during cooling from 1600 °C.

The Ti-doped MgO grains annealed at 900 °C for 5 h showed a bimodal size distribution of the same epitaxial spinel precipitates as indicated by BFI with inset SAED pattern in Fig. 4a and DFI of the spinel in Fig. 4b. Upon this annealing treatment, the primary spinel originally formed during cooling from 1600 °C became about 60 nm in size and the secondary spinel ca. 20 nm in size emerged. A further magnified BFI in Fig. 4c showed that the newly nucleated spinel precipitates were occasionally associated with dislocations. A longer dwelling at 900 °C for up to 30 h caused site saturation and coarsening of parallel-epitaxial spinel precipitates to ca. 50–60 nm in size leaving a precipitate-free zone near the grain boundaries of Ti-doped MgO (Fig. 4d).

The spinel precipitates tended to be equiaxed regardless of firing conditions. The ones ca. 20–25 nm in size newly nucleated at 900 °C for 5 h preferred to form an octahedron, i.e., nearly perfect hexagon in the projection when viewed along [111] zone axis (Fig. 5). Still, there were imperfect cubo-octahedra with {111} and {100} planes running coherently across the Ti-doped MgO/spinel interface decorated with (111) and (001) facets as indicated by the HRTEM image and SAED pattern (Fig. 6). Assuming a $2 \times 2 \times 2$ supercell of rock-salt parent structure and negligible coherency strain, the spinel precipitate would have a lattice parameter of 0.8416 nm given the cell volume (0.4208 nm) of Ti-doped MgO. This is in accord with the mentioned XRD results for the sample fired at 900 °C for 5 h. (A smaller cell lattice parameter than the stoichiometric Mg_2TiO_4 (0.8441 nm) might indicate a Ti-excess composition for the spinel precipitates, although most XRD counts were apparently from intergranular spinel formed by reactive sintering.)

HRTEM image (Fig. 7a) and inverse Fourier transform (Fig. 7b) of Ti-doped MgO also showed G.P. zones parallel to (001) plane, yet with occasional coherency loss to form misfit dislocation as represented by the composite fired at 1600 °C for 4 h. Point count EDX analysis on the areas containing such G.P. zone (Fig. 7c) showed a slight Ti count (ca. 0.5 wt% Ti) and predominant Mg counts from the MgO matrix (ca. 0.3 wt% Ti). These G.P. zones were apparently the relic intermediate phase of the spinel precipitates.

3.3.2. *Intergranular spinel*

In comparison with the spinel precipitates, the larger intergranular spinel formed via reactive sintering showed more clearly the defect microstructures. A

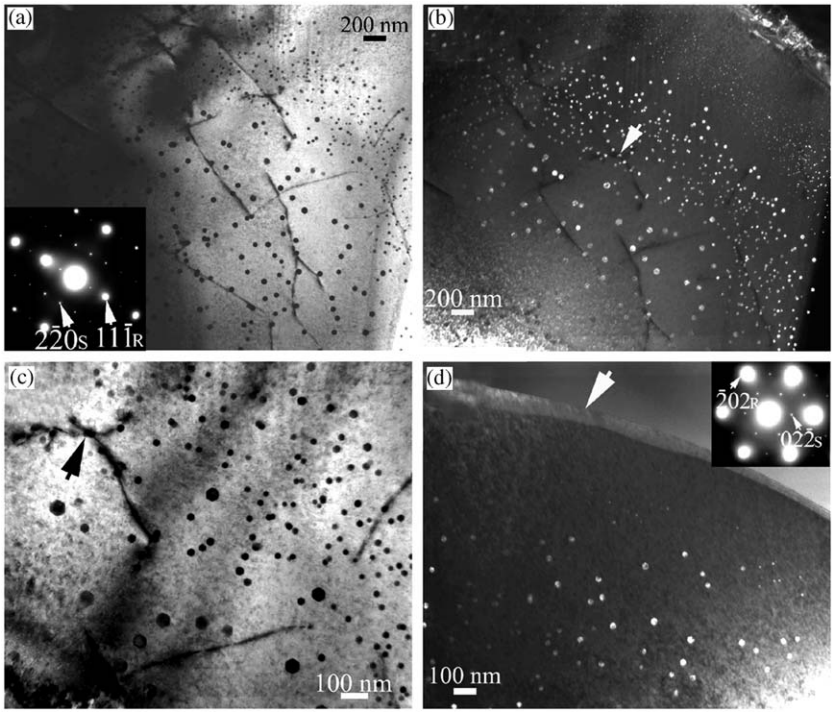

Fig. 4. TEM (a) BFI with inset SAED pattern and (b) DFI ($g = \bar{2}20$ spinel) in [112] zone axis showing bimodal size distribution of spinel precipitates in Ti-doped MgO for MgO/Mg_2TiO_4 composite annealed at 900 °C for 5 h. (c) Magnified BFI from arrow in (b) showing newly nucleated spinel nanoparticles (ca. 20 nm in size) at and away from dislocations (arrow) besides the original ones coarsened to about 60 nm in size. (d) DFI ($g = 02\bar{2}$ spinel) with inset SAED pattern ([111] zone axis) of the sample annealed at 900 °C for 30 h showing uniform size (ca. 50 to 60 nm) distribution of spinel precipitates and precipitate-free zone near grain boundary (arrow).

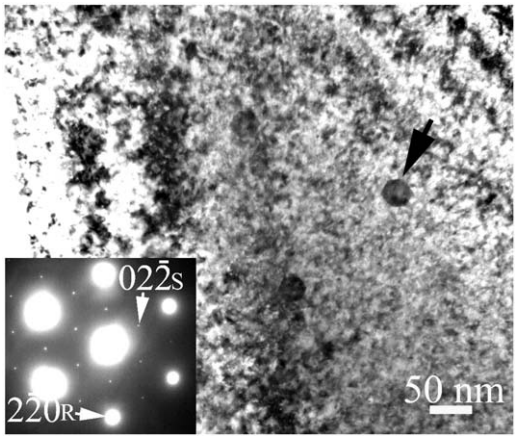

Fig. 5. TEM BFI with inset SAED pattern in [111] zone axis showing nearly perfect hexagon shape of octahedral spinel precipitates (arrow). The spinel was newly nucleated from Ti-doped MgO upon annealing at 900 °C for 5 h.

typical intergranular spinel formed at 1600 °C for 4 h showed complicated diffraction contrast in the BFI yet no extra spots in SAED pattern (Fig. 8a). HRTEM image and reconstructed image by inverse Fourier transform further showed the presence of less intense dots randomly distributed throughout the Mg_2TiO_4 lattice (Fig. 8b). Each dot can represent a column of atoms and so its different intensity than the others means that this column has different content than the other ones and hence it contains, probably, more than one point defect. In other words, this HREM image gives evidence for some disorder and the presence of point defects arranged in line with the direction of the projection. These dots with darker contrast may be attributed to disordering of mixed Mg and Ti cations as discussed later. The intergranular spinel has a composition close to 2:1 Mg/Ti stoichiometry according to point-count EDX analysis (Fig. 8c). However, a smaller lattice parameter (0.8423 nm) than stoichiometric value (0.8441 nm), as mentioned, indicates it is slightly Ti-richer (i.e., $Ti_{1.06(1)}Mg_{1.94(1)}O_4$). It is an open question whether the Ti enrichment in the spinel formed by reactive sintering was a result of approaching equilibrium in the two-phase region at 1600 °C in air [1,2]. Further dwelling at 1600 °C for up to 24 h caused lattice plane modulation and defect clusters as shown by the compiled HRTEM image, SAED pattern and reconstructed image in Fig. 9. The modulation in the image has nothing to do with Moiré fringes because the image was taken from an area free of the MgO, as indicated by SAED pattern inset. In fact, more than 10 independent observations confirmed that such modulation is characteristic of the intergranular spinel.

After annealing at 900 °C for 5–30 h, the intergranular spinel still showed no appreciable dislocations, yet

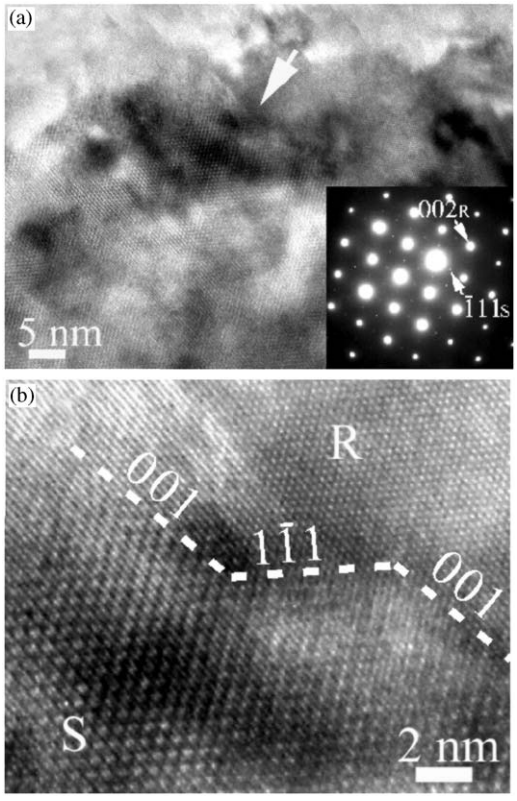

Fig. 6. (a) HRTEM image with inset SAED pattern ([110] zone axis) and (b) further magnified view from area indicated by arrow in (a) showing {111} and {100} planes running coherently across the {111}- and {001}-faceted interface of spinel precipitate (denoted as S) and Ti-doped MgO with rock-salt structure (denoted as R). The same specimen as in Fig. 5.

exhibited diffuse scatter intensity (DSI) along reciprocal $\langle 1\bar{1}0\rangle$ direction as represented by the specimen fired for 30 h (Fig. 10). DSI may be attributed to association of defect dimmers/trimers, short-range ordering and/or eutectoid decomposition as discussed later.

4. Discussion

4.1. Defect chemistry

4.1.1. MgO

MgO is a highly stoichiometric oxide with Mg in a fixed valence. Changes in P_{O_2} alone cause little change in defect concentration in such a solid. The intrinsic defect of MgO is the Schottky type (i.e., cation vacancies and oxygen vacancies in pair) with a formation enthalpy of ~7.7 eV [26]. Such defects can be generated by the following equation [27] in Kröger–Vink notation [28]:

$$\text{null} \xrightarrow{\text{MgO}} V''_{\text{Mg}} + V^{\bullet\bullet}_{\text{O}}. \quad (1)$$

In this notation, the type of imperfection is indicated by a major symbol, the location is described by a subscript, and finally the charge of the defect relative to the normal lattice is indicated by a superscript. Here, null means the creation of defects from a perfect lattice; V''_{Mg} and $V^{\bullet\bullet}_{\text{O}}$ represent a double negatively charged magnesium and oxygen vacancy, respectively.

4.1.2. Ti-doped MgO

Ti^{4+} (0.061 nm) has a smaller ionic size than Mg^{2+} (0.072 nm) in coordination number 6 [29], i.e., in the octahedral sites of the MgO lattice. The charge balance perturbed by the dissolution of Ti^{4+} is expected to create $Ti^{\bullet\bullet}_{\text{Mg}}$, charge compensated by V''_{Mg} through the following reaction:

$$TiO_2 \xrightarrow{\text{MgO}} Ti^{\bullet\bullet}_{\text{Mg}} + V''_{\text{Mg}} + 2O_{\text{O}}. \quad (2)$$

Columbic attraction between $Ti^{\bullet\bullet}_{\text{Mg}}$ and V''_{Mg} may result in association to form a neutral dimmer ($Ti^{\bullet\bullet}_{\text{Mg}} - V''_{\text{Mg}}$). Excess $Ti^{\bullet\bullet}_{\text{Mg}}$ introduced upon cooling/annealing, as manifested by X-ray lattice parameters, may cause further association to form trimers analogous to the case of Fe-doped MgO characterized by high-temperature electron paramagnetic resonance spectroscopy in the range of 600–1200 °C [30]. Kinetic studies of MgO single crystals doped with up to 4300 ppm of Fe below 1200 °C [31] also indicated that the room-temperature defect structure of liquid-nitrogen quenched samples consists of many uniformly dispersed clusters, dimers, trimers, and unassociated Fe^{3+} but very few isolated vacancies.

The undersized Ti^{4+} dopant in the Mg^{2+}site could force Ti^{4+} dopant to enter the interstitial site as T_i^{4+} which then induced charge-compensating cation vacancies and 4:1 defect clusters through the following equation:

$$4TiO_2 \xrightarrow{\text{MgO}} 3Ti^{\bullet\bullet}_{\text{Mg}} + [4V''_{\text{Mg}} + Ti_i^{\bullet\bullet\bullet\bullet} + 2e'] + 8O_{\text{O}}. \quad (3)$$

This reaction is preferred at temperatures higher than 1416 °C with nearly 4% of the Ti occupying the tetrahedral sites [20]. Theoretical calculations [32] indicated that interstitial-tetrahedral dopants can stabilize 4:1 defect clusters in 3d transition metal monoxide, e.g., Mn^{3+}- and Fe^{3+}-based 4:1 clusters in $Co_{1-x}O$ and $Ni_{1-x}O$. The formation of the paracrystalline state of defect clusters and then spinel precipitates in Al-doped $Ni_{1-x}O$ was triggered by change in defect type from clusters with octahedral Al to those with interstitial-tetrahedral Al on decreasing temperature [19]. In the present case of Ti-doped MgO, defect clustering as $Ti^{4+}V_4$ units, i.e., four octahedral magnesium vacancies tetrahedrally coordinated about one Ti^{4+} interstitial, may be rather isolated because no paracrystalline distribution of defect clusters was formed in Ti-doped MgO. In any case, at room temperature, Mg_2TiO_4 spinel would become completely inverse type [33] with 100% of the Ti occupying the octahedral sites.

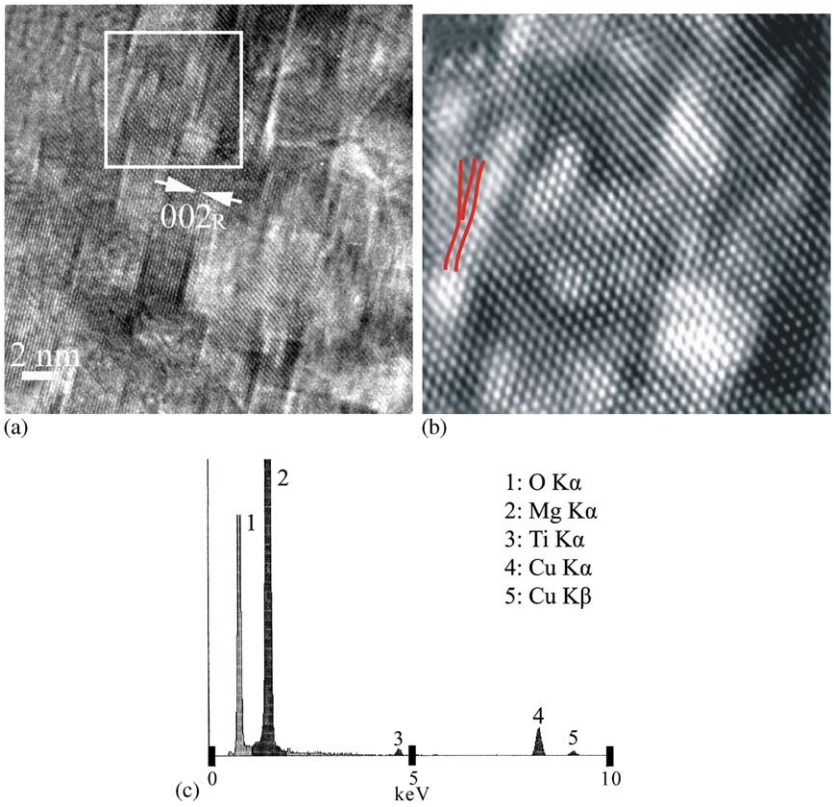

Fig. 7. (a) HRTEM image of Ti-doped MgO and (b) reconstructed image ([110] zone axis) from square region in (a) showing (001)-specific G.P. zone with occasional coherency loss as indicated by the presence of half plane schematically delineated by red lines. (c) Point count EDX spectrum showing considerable Ti and predominant Mg counts from an area covering G.P. zone and Ti-doped MgO matrix. Sample fired at 1600 °C for 4 h followed by quenching in air.

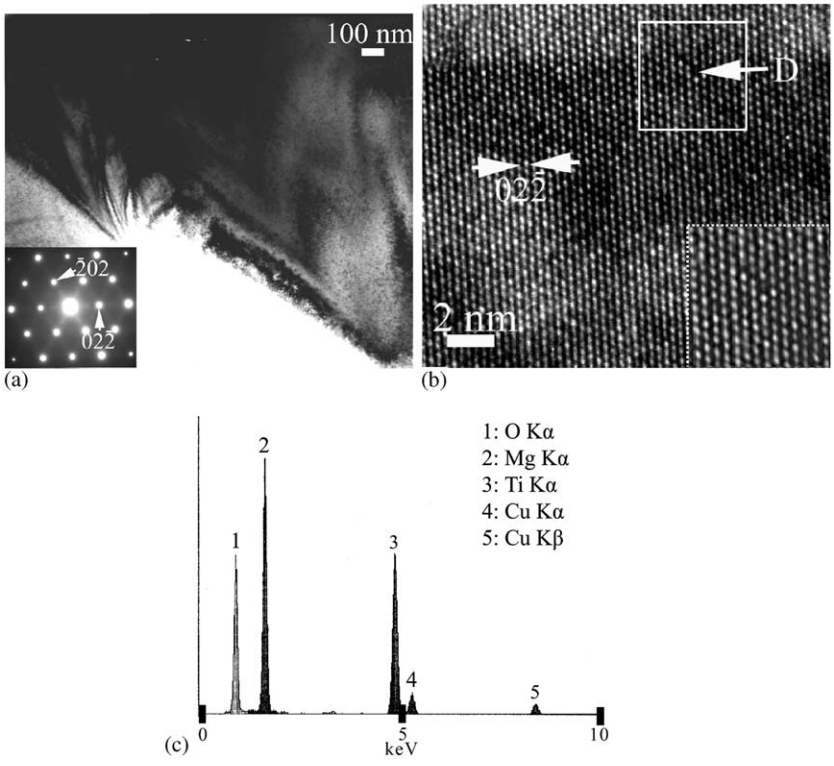

Fig. 8. (a) TEM BFI with inset SAED pattern ([111] zone axis) of the intergranular spinel. (b) HRTEM image with inset reconstructed image (framed with dotted lines) from the square region showing point defects (denoted by D) arranged in line with the direction of the projection and hence a darker contrast in the intergranular spinel. (c) EDX spectrum of the intergranular spinel. The same specimen as in Fig. 7.

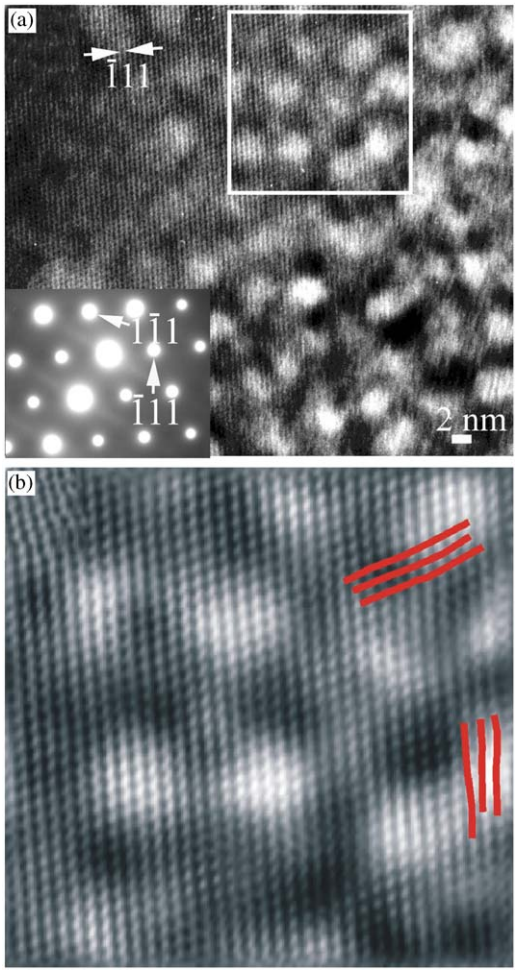

Fig. 9. (a) HRTEM image of the intergranular spinel with inset SAED pattern ([110] zone axis) and (b) reconstructed image from square region in (a), showing *d*-spacing modulation (delineated by red lines) in association with bright areas likely due to defect clusters. Sample fired at 1600 °C for up to 24 h followed by quenching in air.

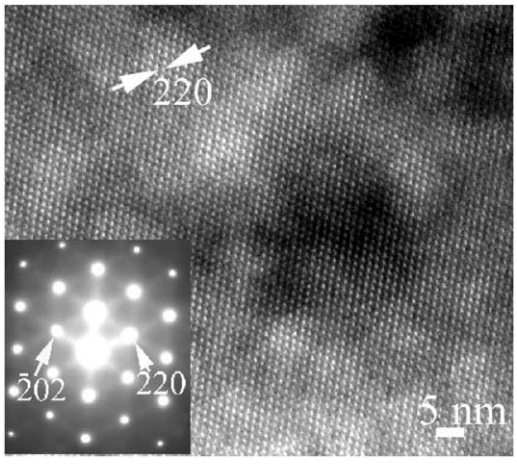

Fig. 10. HRTEM image with inset SAED pattern ([$1\bar{1}1$] zone axis) of intergranular spinel showing DSI along three reciprocal $\langle 1\bar{1}0\rangle$ directions. MgO/Mg_2TiO_4 composite annealed at 900 °C for 30 h followed by quenching in air.

4.2. G.P. zone

Because of a rather limited exsolution upon cooling/annealing, the G.P. zone rather than paracrystalline distribution of defect clusters was a favorable precursor of the Mg_2TiO_4 spinel precipitate. In general, the G.P. zone is coherent with respect to the matrix lattice for a beneficial lower strain energy and interfacial energy as for Cu–Al alloy [3]. The formation of the G.P. zone was believed to involve homogeneous nucleation at vacancies rather than dislocations or grain boundaries for metal alloys. In the present case of Ti^{4+}-doped MgO, the G.P. zone was likely derived from Schottky defects and dimers ($Ti^{\bullet\bullet}_{Mg} - V''_{Mg}$).

As for (*hkl*)-specific G.P. zone, applied stress has been experimentally proved to affect the orientation and shape of the G.P. zone in Cu–Al alloy [5]. In the present composite fired without an applied stress, sintering stress and thermal mismatch of MgO and Mg_2TiO_4 upon cooling may cause preferred orientation of plate-like G.P. zone, and hence single variant of (001)-specific G.P. zone in Ti-doped MgO.

4.3. Controlled nucleation and growth of nano-Mg_2TiO_4 precipitate

In our previous study of $Ni_{1-x}O/NiAl_2O_4$ composite, the platelets of inverse spinel $NiAl_2O_4$ were found to nucleate rapidly at dislocations of Al^{3+}-doped $Ni_{1-x}O$ [19]. Some Al dopant moving from octahedral to interstitial sites below 1200 °C was suggested to cause the spinel nucleation at dislocations. In the present annealing and cooling study of analogue yet more refractory and less solid soluble MgO/Mg_2TiO_4 composite, expulsion of Ti^{4+} caused the formation of (001)-specific G.P. zone under the influence of thermal/sintering stress and then spinel precipitates. The spinel precipitates thus formed were equiaxed, in drastic contrast to plate-like $NiAl_2O_4$ formed at dislocations [19], and controlled to be about 30 nm in size upon cooling from 1600 °C. Further expulsion of small amount of Ti^{4+} at 900 °C resulted in the nucleation of even smaller-sized precipitates at the expense of G.P. zones. Aging for a total of 30 h at 900 °C caused bulk site saturation as manifested by the coarsened precipitates ca. 60 nm in size and a precipitate-free zone at the grain boundaries of Ti-doped MgO. The tiny spinel precipitates have well-developed {111} and {100} facets in order to minimize coherency strain energy and surface energy.

The present study demonstrated that controlled nucleation and growth of nanosize precipitates could be readily achieved in binary oxide system with limited solid solubility and nucleation sites. The metal oxides when tailored as nanosize domains and exposed on the surface of ceramic material may have potential

applications on heterogeneous catalysis for specific chemical/physical properties due to nanosize effect.

4.4. Defects of intergranular Mg_2TiO_4 spinel

The intergranular spinel formed at 1600 °C for 4 h showed the existence of point defects (Fig. 8), which may be attributed to small amount of relic Ti occupying tetrahedral sites by 1416 °C [20]. This interpretation is supported by excess Ti for the intergranular spinel than the stoichiometric Mg_2TiO_4, as indicated by the lattice parameter determined by XRD. When fired at 1600 °C for up to 24 h (Fig. 9), the defect in the intergranular spinel was further complicated by composition modulation and/or defect clusters due to a progressively Ti-richer composition away from stoichiometric Mg_2TiO_4.

Further annealing at 900 °C caused DSI along reciprocal $\langle 1\bar{1}0\rangle$ directions for the intergranular spinel. The DSI can hardly be attributed to long-range ordering, such as distortion into tetragonal symmetry (space group $P4_122$) below 664 °C [21]; however, it can be rationalized by the possible presence of defect dimmers/trimers as a result of short-range ordering of mixed Mg and Ti occupying octahedral sites and Mg vacancies. In fact, analogous ordering behavior has been reported for parent rock-salt structure with trivalent dopant such as Fe^{3+}-doped MgO [30,34–35]. It is an open question whether DSI has anything to do with the possible onset decomposition toward even Ti-richer composition upon aging near subsolidus eutectoid decomposition temperature. In this regard, decomposition of magnesium titanate spinel to $MgTiO_3$ plus MgO was thermodynamically predicted to occur around 900 °C [2] and experimentally proved by prolonged annealing at 480 °C under ambient pressure [36]. The $T-P$ equilibrium phase boundary of this decomposition reaction was determined by static compression experiment to be $P(\text{kbar}) = -18 + 0.019\,T\,(^\circ\text{C})$ [37]. A positive dT/dP slope of this equation suggests a higher decomposition temperature at a higher pressure. The Mg_2TiO_4 precipitates embedded in MgO matrix with additional nanophase effect (i.e., capillary force) may thus be more difficult to decompose, in comparison to much larger-sized intergranular spinel. Future studies of MgO/Mg_2TiO_4 composites at temperatures lower than 900 °C are required to clarify this point. It is also of interest to study whether long-range ordering accompanied with cubic to tetragonal transformation [21] results in domain boundaries and/or twin variants for Mg_2TiO_4.

5. Conclusions

1. Mg_2TiO_4 spinel particles, having nanosized and well-developed {111} and {100} facets, were precipitated from MgO with a rather limited solid solubility of Ti when the sintered MgO/Mg_2TiO_4 composites were cooled from 1600 °C in air.
2. Even smaller-sized Mg_2TiO_4 spinel particles were precipitated in MgO when the composites were subjected to annealing at 900 °C for specific time period.
3. There is a precipitate-free zone at the grain boundaries due to preferred bulk nucleation sites.
4. The intergranular spinel showed $\langle 110\rangle$-specific diffuse scattering intensity, which can be attributed to short-range ordering and/or onset decomposition.

Acknowledgments

This research was supported by National Science Council, Taiwan, ROC under contract NSC93-2216-E-110-014 and partly by Center for Nanoscience and Nanotechnology at NSYSU. We thank anonymous referees for constructive comments.

References

[1] I. Shindo, J. Crystal Growth 50 (1980) 839–851.
[2] B.A. Wechsler, A. Navrotsky, J. Solid State Chem. 55 (1984) 165–180.
[3] D.A. Porter, E.A. Easterling, Phase Transformations in Metals and Alloys, second ed, Van Nostrand Reinhold, New York, 1992.
[4] M.L. Wu, D. Gan, P. Shen, Mater. Sci. Eng. A 297 (2001) 119–123.
[5] T. Eto, A. Sato, T. Mori, Acta Metall. 26 (1978) 499–508.
[6] T.R. Welberry, A.G. Christy, J. Solid State Chem. 117 (1995) 398–406.
[7] B.E.F. Fender, F.D. Riley, in: L. Eyring, M. O'Keefe (Eds.), The Chemistry of Extended Defects in Non-Metallic Solids, North-Holland, Amsterdam, 1970.
[8] C.R.A. Catlow, B.E.F. Fender, J. Phys. C: Solid State Phys. 8 (1975) 3267–3279.
[9] T.R. Welberry, A.G. Christy, Phys. Chem. Miner. 24 (1997) 24–38.
[10] P. Vallet, P. Raccah, Mem. Sci. Rev. Metall. 62 (1965) 1–29.
[11] B. Andersson, J.O. Sletnes, Acta Crystallogr. Sect. A 33 (1977) 268–276.
[12] H.G. Sockel, H. Schmalzried, Ber. Bunsenges. Phys. Chem. 72 (1968) 745–754.
[13] P. Shen, S. Chen, H.S. Liu, Mater. Sci. Eng. A 161 (1993) 135–143.
[14] J. Chen, P. Shen, J. Solid State Chem. 140 (1998) 361–370.
[15] S.M. Tomlinson, C.R.A. Catlow, J.H. Harding, J. Phys. Chem. Solids 51 (1990) 477–506.
[16] M. Oku, Y. Sato, Appl. Surf. Sci. 55 (1992) 37–41.
[17] K.T. Lin, P. Shen, J. Solid State Chem. 145 (1999) 739–750.
[18] W.H. Lee, P. Shen, J. Solid State Chem. 177 (2004) 101–108.
[19] S.R. Wang, P. Shen, J. Solid State Chem. 140 (1998) 38–45.
[20] H.St.C. O'Neill, S.A.T. Redfern, S. Kesson, S. Short, Am. Miner. 88 (2003) 860–865.
[21] R.L. Millard, R.C. Peterson, B.K. Hunter, Am. Miner. 80 (1995) 885–896.
[22] M.H. Lewis, Philos. Mag. 13 (1966) 777–794.

[23] Y.B. Lee, H.C. Park, K.D. Oh, F.L. Riley, J. Mater. Sci. 33 (1998) 4321–4325.
[24] D.B. Williams, Practical Analytical Electron Microscopy in Materials Science, Philips Electronic Instruments, Mahwah, 1984.
[25] B.A. Wechsler, R.B. Von Dreele, Acta Crystallogr. B 45 (1989) 542–549.
[26] Y.M. Chiang, D. Birnie III, W.D. Kingery, Physical Ceramics, Wiley, New York, 1997.
[27] A.E. Hughes, B. Henderson, in: J.H. Crawford, L.M. Slifkin (Eds.), Point Defects in Solids, vol. 1, Plenum Press, New York, 1972.
[28] F.A. Kröger, H.J. Vink, Solid State Phys. 3 (1956) 307–435.
[29] R.D. Shannon, Acta Crystallogr. A 32 (1976) 751–767.
[30] T.A. Yager, W.D. Kingery, J. Mater. Sci. 16 (1981) 489–494.
[31] T.A. Yager, W.D. Kingery, Defect Association in MgO, in: W.D. Kingery (Ed.), Advances in Ceramics, vol. 10: Structure and Properties of MgO and Al_2O_3 Ceramics, American Ceramic Society, Columbus, OH, 1984, pp. 139–151.
[32] R.W. Grime, A.B. Anderson, A.H. Heuer, J. Phys. Chem. Solids 48 (1) (1987) 45–50.
[33] M.T. Weller, Inorganic Materials Chemistry, Oxford University Press, New York, 1994, pp. 1–92.
[34] W.H. Gourdin, W.D. Kingery, J. Mater. Sci. 14 (1979) 2053–2073.
[35] T.A. Yager, W.D. Kingery, J. Am. Ceram. Soc. 65 (1982) 12–15.
[36] P. Delamoye, A. Michel, CR Acad. Sci. Ser. C 269 (1969) 837–838.
[37] S. Akimoto, Y. Syono, J. Chem. Phys. 47 (1967) 1813–1817.